STEEL/VISCOELASTIC/STEEL SANDWICH SHELLS COMPUTATIONAL METHODS AND EXPERIMENTAL VALIDATIONS

Anne-Sophie Plouin and **Etienne Balmès**

École Centrale Paris

MSSMat

92295 Châtenay-Malabry, France

ABSTRACT

Constrained viscoelastic layers have traditionally been considered as damping enhancement mechanisms. The recent large scale availability of steel/viscoelastic/steel sandwich plates has however renewed the need for analysis methods allowing accurate predictions of their dynamic response. A modeling methodology is presented that uses basic shell and solid elements in conjunction with experimentally derived viscoelastic constitutive laws. The choice not to use parametric models (rational fraction, fractional derivatives, ...), while simplifying model characterization and allowing the use of standard finite element codes, leads to models that are really frequency dependent and are thus associated with very high computational costs. Appropriate model reduction, error estimation and pole estimation methods are thus introduced with care taken to allow studies of the frequency/temperature dependence. The proposed methodology is validated for both flat and curved test samples of *Usinor Solconfort* steel/viscoelastic/steel sandwiches.

1 INTRODUCTION

Constrained viscoelastic layers have traditionally been considered as damping enhancement mechanisms. The recent large scale availability of steel/viscoelastic/steel sandwich plates has however renewed the need for analysis methods allowing accurate predictions of their dynamic response.

Rather than seeking time domain methods allowing the use of standard complex eigenvalue solvers (see [5–7] for example), it was chosen to work in the frequency domain with experimentally derived viscoelastic constitutive laws and the motivation for doing so is discussed in 2.1.

Section 2.2 summarizes previous results [9] on the validity of the shell-solid-shell model used to represent sandwiches.

While the exact solution can be computed for a few frequency/temperature points, design studies for industrial structures require many points which would take days or weeks of CPU time. Reduction methods generalizing modal analysis methods to the case of frequency dependent matrices are thus essential. Section 3 summarizes methods proposed in earlier work and addresses error evaluation and pole estimation issues.

The application section 4 first presents an excellent test/analysis correlation for a flat sample of *Usinor Solconfort*. The validity of the proposed computationnal methodology is then evaluated for the model of a press-formed cup with an emphasis on accurately predicting responses on large temperature ranges.

2 MODELING OF METAL/VISCOELASTIC/METAL SANDWICH PLATES

2.1 Characterization of viscoelastic materials

Viscoelastic materials are characterized by a complex frequency and temperature dependent complex modulus E as usual in linear viscoelasticity [1, 2]. Considering the relation between frequency and temperature, the storage modulus E' and the loss factor η are thus given as a function of $\omega\alpha_T$, where α_T, the temperature shift factor, is an absolute function of temperature [3]

$$E(\omega,T) = E'(\omega\alpha_T)(1+j\eta(\omega\alpha_T)) \tag{1}$$

The viscoelastic properties are thus fully characterized by a master curve at a nominal temperature and a law for the evolution of α_T. The viscoelastic considered in this study is the TA resin considered by Usinor for the production of Solconfort sandwich steel. The master curve is shown in figure 1 and a model of the form $\text{Log}(\alpha_T) = -c_1(T-T_0)/(T-T_\infty)$ is used for the temperature shift factor. This paper considers a non-parametric description of the complex modulus which allows the direct use of an experimentally derived master curve. To obtain the modulus at an arbitrary frequency/temperature pair, $\omega\alpha_T$ is first computed and the modulus is estimated using the two nearest points of the master curve and a log-scale linear interpolation. This clearly implies preprocessing of the master curve raw data to obtain a smooth curve, which is equivalent to using higher order interpolation.

Parametric descriptions of the master curves are also fairly classical. Thus the standard viscoelastic solid [1] uses

$$E(s) = E_0\frac{1+\beta s}{1+\alpha s} \tag{2}$$

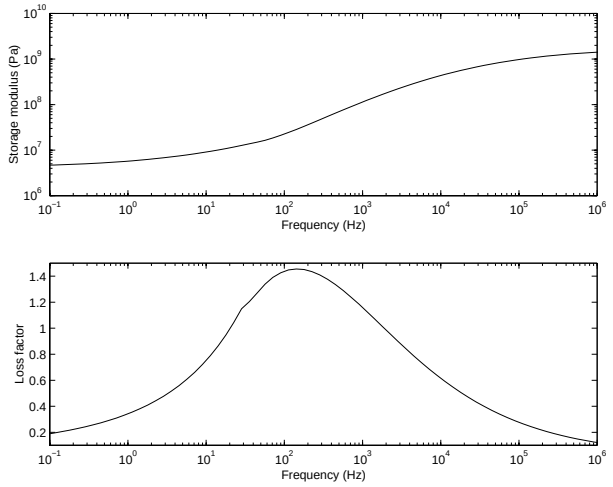

Figure 1: Solconfort-TA master curve at $20^\circ C$

where α is known as the constant of stress relaxation and β is a constant of the model. However, the use of this model is limited by its incapacity to describe a real material behavior over a wide frequency range. Well known alternatives to the standard viscoelastic solid, are the fractional derivative model [4]

$$E(s) = E_0 \frac{1 + \sum_i a_i (s)^{\beta_i}}{1 + \sum_i b_i (s)^{\alpha_i}}, \text{ with } 0 < \alpha_n, \beta_n < 1 \qquad (3)$$

known for its wide frequency range of validity but difficult to represent in the time domain. The GHM (from Golla-Hughes-McTavish [5, 6])

$$sG(s) = G_0 \left(1 + \sum_i \alpha_i \frac{s(s+2\zeta_i\hat{\omega}_i)}{s^2+2\zeta_i\hat{\omega}_i s+\hat{\omega}_i^2} \right), \qquad (4)$$

and ADF (Anelastic Displacement Fields [7])

$$G(s) = G_0 \left(1 + \sum_i \Delta_i \frac{s}{\Omega_i+s} \right). \qquad (5)$$

have published time domain equivalents and have been used in many applications.

These applications rarely acknowledge that both the GHM and ADF models use constitutive laws that correspond to chains of 3 parameter standard viscoelastic models (called Kelvin chain models in [1]) so that the two methods mostly differ in how they formulate the equivalent time domain representation (using the Kelvin chain model, one can easily determine when they are expected to give strictly identical predictions).

The logic for not using the parametric approach is the following. Industrial size models have large number of Degrees of Freedom (DOFs), so that vibration studies are almost always performed using modal bases. Expressing parametric viscoelastic constitutive laws in the time domain, multiplies the number of DOFs in the model at least by the number of time derivatives / real poles in the constitutive law. This leads to huge models even for fairly trivial structures, requires the experimental determination of the coefficients, does not apply for fractional derivative models, and requires the use of complex eigenvalue solvers with repeated solutions needed at each temperature.

Directly working in the frequency domain, with arbitrary constitutive laws, implies that no algorithm is readily available to compute modes but leads to much smaller models. Computing the exact solution at each frequency/temperature point is still not acceptable so that advances in model reduction methods are needed and discussed in section 3. Building a time domain modal model is a second difficulty that is not addressed in this paper.

2.2 The 3L*ayer* shell/solid/shell finite element model

The modeling of sandwich plates with two stiff shells bonded together by a very soft viscoelastic material is a difficult subject. Composite plate models cannot be used because they fail to represent the strong variations of in plane strains through the thickness. Developing a specific element is a tough subject and will not be easily implemented in commercial FEM codes. As shown in figure 2, the approach retained here is to use two classical shell elements for the stiff layers and a standard volume element for the viscoelastic material. For the stiff layers, the element nodes are off-set to the plane in contact with the viscoelastic instead of the standard mid-plane. This results in coincident nodes and thus the proper coupling.

This approach doubles the number of DOFs that would be used for a classical thick shell formulation, but the addition of DOFs is compensated by reduction techniques described in section 3. Standard meshes for the stiff layers lead to very

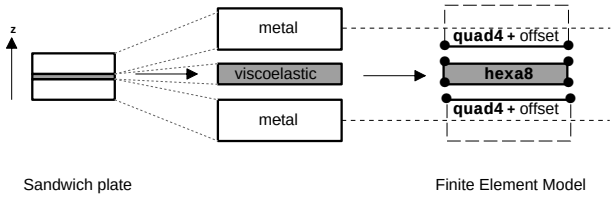

Figure 2: The 3L shell/solid/shell element construction

poor aspect ratios for the volume element so that one can question the validity of its formulation. In particular, when using 4 node shells and thus 8 node volumes, it is known that 8 node volumes have a tendency to lock when subjected to bending. The experience of the authors, illustrated in Ref. [9], is that, for the applications of interest where the core is very much softer than sides, the energy in the viscoelastic is almost exclusively linked to shear deformation. The element does

lock but this locking has no impact on the predicted response. In this application, it is thus acceptable to use volumes with very poor aspect ratios.

For this study, the `quad4` thick shell element of the SDT [8] is used. This element uses a `Q4WT` formulation for the membrane and a `Q4Gamma` formulation for bending. The 3L model thus leads to a 4-node/48-DOF element defined in the upper or lower plane of the viscoelastic layer.

3 REDUCTION METHODS FOR VISCOELASTIC MODELS

This section describes model reduction techniques to obtain reasonable computational costs and used in this study. For the examples, one will only consider a single type of viscoelastic material while the rest of the structure is assumed to be elastic. The form of the input/output model is thus

$$\begin{array}{c}\left[-M\omega^2+K_e+E_v(\omega)K_v\right]\{q(\omega)\}=[b]\{u(\omega)\}\\ \{y(\omega)\}=[c]\{q(\omega)\}\end{array} \quad (6)$$

where M, the mass matrix, K_e, the elastic part of the stiffness matrix, and K_v, the viscoelastic part for a unit Young's modulus E_v, are of size $N \times N$.

3.1 Basic model projection

Reduced model approaches compute frequency responses by projecting the model (6) on a basis $[T]$, with the assumption that $\{q\} \simeq [T]\{q_R\}$. The projection of model on the considered basis leads to a low order model (as many generalized DOFs as independent columns in the matrix T)

$$\begin{array}{c}\left[-T^TMT\omega^2+T^TK(\omega)T\right]\{q_R(\omega)\}=\left[T^Tb\right]\{u(\omega)\}\\ \{y(\omega)\}=[c]\{q_R(\omega)\}\end{array} \quad (7)$$

For elastic models (real and frequency independent stiffness matrix), the standard reduction basis combines normal modes and a static correction to the considered load $\left[K^{-1}[b]\right]$.

Normal modes are solution of the eigenvalue problem

$$\left[-M\omega_j^2+K\right]\phi_j=0. \quad (8)$$

and one retains the low frequency modes covering the frequency range of interest. The static correction $\left[K^{-1}[b]\right]$ is introduced to ensure a correct representation of the low frequency contribution of truncated high frequency modes.

This projection when applied to a viscously damped model ($K(\omega) = K + i\omega C$) leads to diagonal mass and stiffness matrices (orthogonality conditions associated to the eigenvalue problem (8) and a fully populated damping matrix. The assumptions of proportional or modal damping use models where off-diagonal terms in T^TCT are zero. These assumptions are valid for low damping [10, 11] and are thus of little interest here.

For cases where the real part of the stiffness is frequency and temperature dependent, the projection (7) can still be used directly but the standard basis with normal modes and static correction is insufficient to obtain correct predictions.

3.2 Reduction of viscoelastic models

As the normal modes are not defined for a frequency dependent stiffness matrix, the projection described in section 3.1 can be applied by replacing the normal modes by either a multi-model approach [12] or the pseudo-normal modes [13]. The multi-model approach consists in taking normal modes computed for the value of the real part of the stiffness at one or two frequencies [12], for instance

$$\left[\begin{array}{cc}\Phi(E(\omega_{min})) & \Phi(E(\omega_{max}))\end{array}\right] \quad (9)$$

The pseudo-normal modes $\tilde{\phi}_{j=1,NR}$ are defined as the solutions of the generalized eigenvalue problem

$$\left[-M\tilde{\omega}_j^2+\mathsf{Re}(K(\tilde{\omega}_j))\right]\tilde{\phi}_j=0 \quad (10)$$

As for standard spectral approximations, keeping an approximation of the contribution of high frequency modes can be important. The bases (9) or (10) thus need to be complemented by a term similar to the static correction used for elastic structures. To introduce this correction, one defines a reference stiffness K_0 (taken here to be $[K_0] = [K_e + \mathsf{Re}(E(\omega_{\max}))K_v]$ with no very convincing justification) and adds to the basis a static correction defined by

$$[T_A] = [K_0]^{-1}[b]. \quad (11)$$

Damping effects are significant in the considered applications, so that not taking into account the imaginary part of the dynamic stiffness may limit the achievable accuracy. A first order correction is thus added to the initial basis. If the normal modes are used, one computes the static response to the load generated by the imaginary part of the stiffness when exciting a given pseudo-normal mode

$$\left[\tilde{T}_{Cj}\right] = [K_e + \mathsf{Re}(E(\tilde{\omega}_j))K_v]^{-1}[K_v]\left\{\tilde{\phi}_j\right\}. \quad (12)$$

If a multi-model is used, ones computes the static response to the load generated by the imaginary part of the stiffness when exciting the set of chosen normal modes for the real part of a constant stiffness

$$[T_C] = [K_0]^{-1}[K_v][\Phi(E(\omega_{min}))\ \ \Phi(E(\omega_{max}))]. \quad (13)$$

To generate a unique basis allowing the predictions of FRFs for different temperatures, it is clear that the pseudo-normal modes cannot be used anymore. The multi-model method is thus retained.

3.3 Error estimation

As for all linear system, the resolution of the first equation of model (6) allows to build the residue characteristic of the error made with the approximation of the true solution by the reduced solution $\{q_R\}$. For the reduced solution

$$\{q_R(\omega)\} = \left[T^TZ(\omega)T\right]^{-1}\left[T^Tb\right]\{u(\omega)\} \quad (14)$$

the residue, which gives a direct indication of the error associated with the reduced solution, is expressed as

$$\hat{R}(\omega) = [Z(\omega)][T]\{q_R(\omega)\} - [b]\{u(\omega)\} \tag{15}$$

In practice, one uses $u(\omega) = 1$. An important issue for an error estimation is to choose a norm for the residue. The euclidean norm is not physically based and would be sensitive to unit or mesh density changes. Strain or kinetic energy are the standard, physically motivated choices [?]. Since the residue (15) has the dimension of an effort, one must associate it with a displacement. To do so, one considers a reference stiffness $[K_0]$ (here the real part of the stiffness at low moduli) and computes the static response to the residue

$$R(\omega) = [K_0]^{-1}\hat{R}(\omega) \tag{16}$$

The error estimate is then the ratio of the strain energy of the displacement residue (16) and that of the response

$$\varepsilon(w,T,b) \quad = \quad \frac{\left\{\overline{R}\right\}^T[K_0]\{R\}}{\left\{\overline{Tq_R}\right\}^T[K_0]\{Tq_R\}} \tag{17}$$

An iterative methodology to increase the accuracy of any reduction basis is to enrich the initial basis with the displacement residues $[R]$

$$\left[T^{k+1}\right] = \left[T^k \;\; \mathsf{Re}(R_{selected}) \;\; \mathsf{Im}(R_{selected})\right] \tag{18}$$

where a methodology to select the frequency/temperature pairs at which the residues are computed is clearly needed.

The approach retained in this paper is close to the idea of modal filters. The reduction basis is first orthonormalized with respect to M and K_0 so that each generalized coordinate corresponds to a modal coordinate of the reference model. Since mode shapes of the viscoelastic model strongly related to the reference ones, the frequency response functions

$$H_k(\omega) = [\delta_k]^T\left[T^T Z(\omega) T\right]^{-1}[\delta_k] \tag{19}$$

mostly show a single peak. The results shown in the application section are based on an automated identification algorithm (based on [?]) that uses these FRFs to estimate the frequency and damping associated with the complex mode that contributes most to each FRF.

The energy error is then evaluated at the frequencies estimated for the low frequency viscoelastic modes.

4 APPLICATIONS

4.1 Test/analysis correlation on flat samples

To validate the reduction model methodology, computations were carried out on rectangular $30 \times 300mm$ sandwich plates in the $100 - 1500Hz$ frequency band for the $10 - 40^\circ C$ temperature range. The thickness are $0.7mm$ for the steel sides and $0.05mm$ for the viscoelastic layer. The elastic properties taken for the steel sides are $E = 2.2\ 10^{11}N/m^2$, $\nu = 0.3$ and $\rho = 7.8\ 10^3 kg/m^3$. The viscoelastic is the Solconfort-TA resin whose damping properties given by the master curve in figure 1. The finite element model uses 2460 DOFs, 205 nodes, 160 elements of 3L model described in section 2.2.

The high modulus ($1500Hz/10^\circ C$) stiffness is used as the reference K_0. The considered reduction basis combines the first 19 normal modes for a low modulus ($100Hz/40^\circ C$) stiffness (modes below 2000 Hz), the first 14 normal modes associated with K_0, the static correction (11) and first order correction for damping effects (13). The validity of this basis is checked using the energy ratio (17) and a final prediction using an iteration of the form (18). The final basis $\left[T^f\right]$ leads to a basis containing 51 vectors.

For an input and an output in the center of the plate, experimental FRFs provided by Usinor and FRFs obtained with the reduction basis $\left[T^f\right]$ are compared in figure 3 at 10, 20, 30 and $40^\circ C$. Except a slight shift at the anti-resonances, the match is excellent at all temperatures. These results encouraged us to pursue the work with pressed-formed component models.

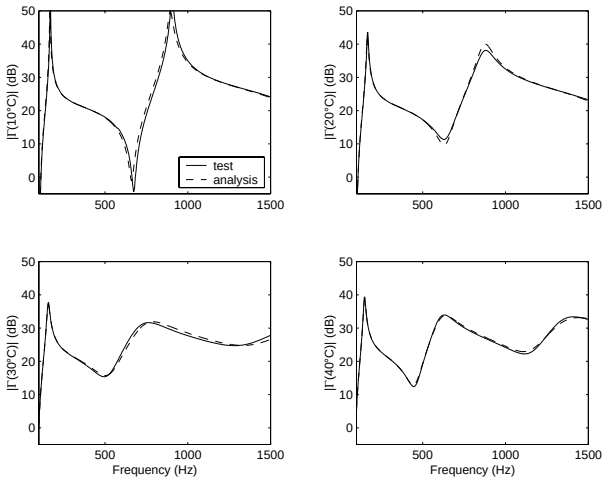

Figure 3: Frequency response functions at 10, 20, 30 and $40^\circ C$

4.2 Application to pressed-formed component models

One now considers press formed steel/viscoelastic/steel "cups" shown Figure 4. The base radius of one cup is $0.10m$, its $0.05m$, its edge $0.04m$. The generator of the curved parts is a quadrant of $0.01m$ radius. The thicknesses are $0.7mm$ for the steel sides and $0.045mm$ for the viscoelastic layer. The elastic properties taken for the steel sides are identical to those of the flat samples described in section 4.1.

The finite element model used in this study is shown in Figure 4. The model uses 10812 DOFs, 901 nodes, 864 4-node

and 36 3-node 3l elements of 3L described in section 2.2.

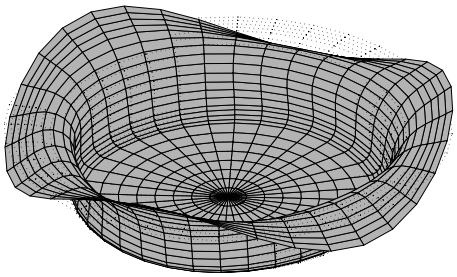

Figure 4: Finite element model of the components

To predict the frequency response functions in the $300 - 1500Hz$ frequency band, 4 reduction basis were considered. **Model A** contains the normal modes associated to the low modulus and the static correction ($[K_0]$ computed for the modulus at $1500Hz/0^\circ C$)

$$[T_{\mathcal{A}}] = \left[\begin{array}{cc} \Phi(E_{min}) & K_0^{-1}b \end{array} \right] \tag{20}$$

Model B, compared to model A, contains an additional set of normal modes associated to the high modulus stiffness $[K_0]$

$$[T_{\mathcal{B}}] = \left[\begin{array}{ccc} \Phi(E_{min}) & \Phi(E_{max}) & K_0^{-1}b \end{array} \right] \tag{21}$$

Model C adds to model B the first order correction for the damping effects

$$[T_{\mathcal{C}}] = \left[\begin{array}{cc} T_{\mathcal{B}} & K_0^{-1}K_v\Phi(E_{max}) \end{array} \right] \tag{22}$$

Model D, compared to model C, introduces the correction associated to displacement residues $[R]$

$$[T_{\mathcal{D}}] = \left[\begin{array}{ccc} T_{\mathcal{C}} & \mathsf{Re}\left(K_0^{-1}R\right) & \mathsf{Im}\left(K_0^{-1}R\right) \end{array} \right] \tag{23}$$

The residues are computed at the first ten estimated viscoelastic frequencies, leading to a final basis with 109 vectors.

To compare models A, B, C and D, predictions were carried out for temperatures between 0 and $40^\circ C$. For each model and temperature, the FRFs described by equation (19) were computed and the error was evaluated at the estimated modal frequencies. Figure 5 shows, for each model as a function of temperature, the evolution of the first three distinct frequencies and the associated errors.

Frequencies decrease with temperature, which is expected since the viscoelastic becomes softer. The figure shows decreases of 34% which clearly indicates the need to take temperature into account.

Model A gives very poor predictions in most cases with difficulties just to estimate the second and third frequencies.

For temperatures above $15^\circ C$, model B gives frequencies comparable to model C while the error, similar to model C for the second and third frequencies, is much higher for the

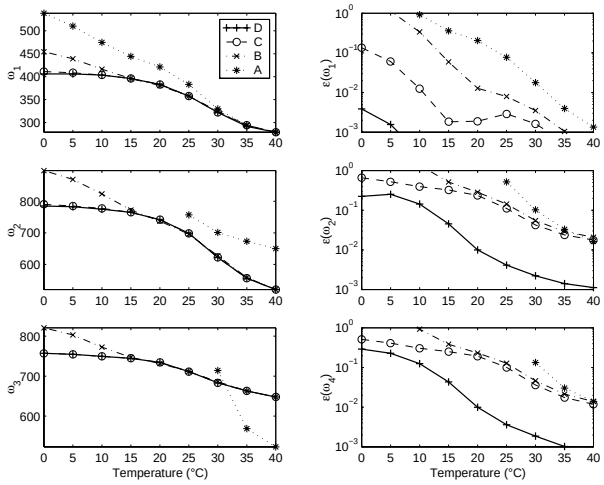

Figure 5: (left) First 3 frequencies ω_j, (right) Error in energy $\varepsilon(\omega_j)$

first frequency (still above 6% at $15^\circ C$). For temperatures below $15^\circ C$, model B is clearly inaccurate. The frequencies are overpredicted and the error exceed 100% for the lowest temperature.

Model C gives frequencies very close to the frequencies of model D but the error computed at these frequencies is higher specially for the high temperatures. For the first frequency, the error is maximum (13%) at $0^\circ C$ and decreases below 1% from $15^\circ C$. For the two last frequencies, the error is maximum (above 60%) at $0^\circ C$ and decreases until approximatively 1.5% at $40^\circ C$.

As expected, model D presents the lowest error for the three modes and all temperatures. The error at the first resonance frequencies is below 0.5% for all temperatures. For the two other frequencies, the error is maximum (approximately 30%) at $0^\circ C$ and decreases below 1% above $20^\circ C$. The residues used to go from model C to model D are for each mode the the residue at the temperature where the error is largest. For all frequencies, the maximum error occurs at $0^\circ C$ which corresponds to the high modulus. The relatively high energy errors at low temperatures, thus still need to be explained.

Figures 6-7 show force to acceleration transfer functions for the 4 reduction bases and different temperatures. Model A is inaccurate compared to the other models for temperatures below $35^\circ C$. However, this model is comparable to model B for temperature above $35^\circ C$ as expected. Indeed, these temperature corresponds the range of low viscoelastic moduli and the normal modes chosen for the reduction basis are associated to a stiffness matrix computed with a low viscoelastic modulus. Models B gives similar results to models C starting at $20^\circ C$ but, below this temperature, it mismatches resonances and anti-resonances. Model C predicts the same resonance frequencies as model D with a slight difference of amplitudes but the accuracy on the anti-resonances decreases significantly

with temperature.

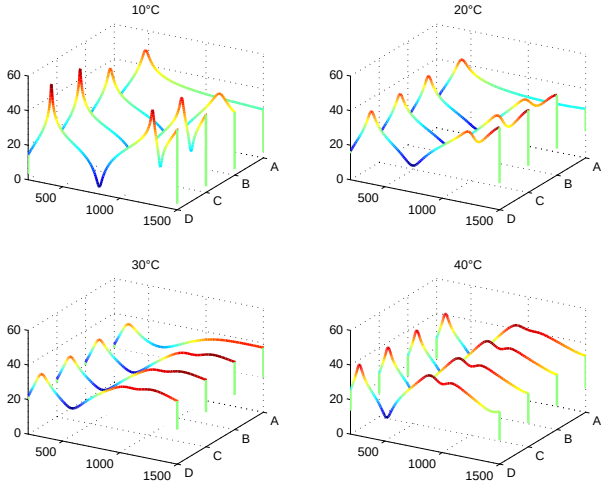

Figure 6: Frequency response functions

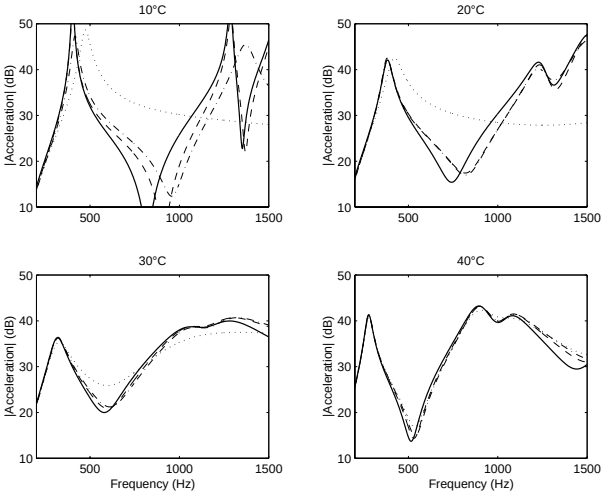

Figure 7: Frequency response functions: (—) model D, (−−) model C, ($\cdot-\cdot$) model B, ($\cdots$) model A

As the FRFs are heavily damped, they only allow an accurate evaluation of the influence of temperature and reduction basis selection on the few well separated peaks. The modal filter technique gives estimates of the poles which are illustrated in figure 8. An interesting feature is the frequency crossing near $20°C$. On the left, one shows the location of the poles of model D in the complex plane. This plot indicates that maximum damping is obtained near $30°C$ for all modes. The frequency crossing near $20°C$ does not correspond to a pole crossing.

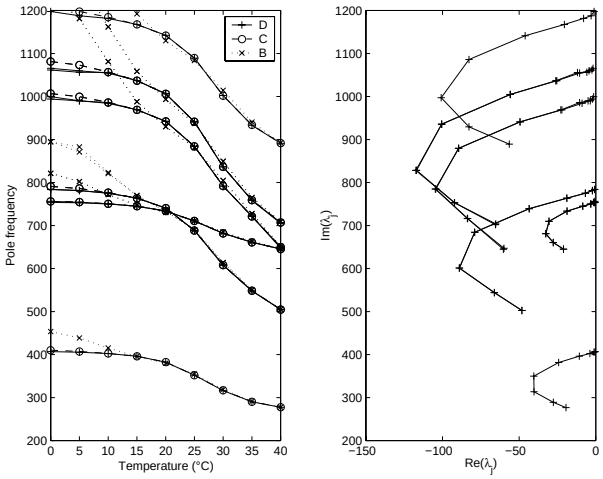

Figure 8: (left) Pole frequencies ω_j, (right) Poles λ_j in complex plane for model D

The decision on which model to use, must also take computational times into account. Table 1 indicates approximate time decompositions. The 77.8 s needed for a full order FRF point clearly motivate the need for model reduction : computing a few thousand points at several temperatures would take days. The construction of model reduction bases is a significant effort that is comparable to computing a few full order frequency points. Once the reduced model built however, one can easily evaluate responses for a large number of frequency/temperature points.

	CPU time (s)
assembly	104
30 normal modes	330
model A basis (49 modes)	3.56
reduced FRF/frq point	9.9e-3
model B basis (72 modes)	3.8
reduced FRF/frq point	20e-3
model C basis (97 modes)	24.1
reduced FRF/frq point	39e-3
model D basis (109 modes)	47.5
reduced FRF/frq point	60e-3
full FRF/frq point	77.8

TABLE 1: CPU times FRF predictions using SDT 3.1 [8] on a SGI R10000 processor

5 CONCLUSION

The paper has presented a complete methodology allowing the practical study of frequency/temperature dependence of large finite element models with viscoelastic materials without restrictions on the form of the constitutive law. The validity of computations was demonstrated for both flat and curved

components. Remaining needs are linked to the refinement of the error evaluation strategy and the ability to automatically build equivalent time domain representations.

Excellent test/analysis correlation was shown for flat components. Similar comparisons on press formed components have not given as good results and difficulties are currently assumed to be linked to improper material characterization.

Acknowledgment : the experimental results used in this paper were kindly provided by P. Lorenzini of USINOR Recherche (Florange, France)

REFERENCES

[1] **Bert, C.**, *Material Damping: An Introductory Review of Mathematical Models, Measures, and Experimental Techniques*, Journal of Sound and Vibration, Vol. 29, No. 2, pp. 129–153, 1973.

[2] **Salençon, J.**, Viscoélasticité, Presse des Ponts et Chaussés, Paris, 1983.

[3] **Nashif, A., Jones, D.** and **Henderson, J.**, Vibration Damping, John Wiley and Sons, 1985.

[4] **Bagley, L.** and **Torvik, P.**, *Fractional calculus - A different approach to the analysis of viscoelastically damped structures*, AIAA Journal, Vol. 21, No. 5, pp. 741–748, 1983.

[5] **Golla, D.** and **Hugues, P.**, *Dynamics of Viscoelastic Structures - A Time-Domain, Finite Element Formulation*, J. of Applied Mechanics, Vol. 52, No. 1, pp. 897–906, dec 1985.

[6] **McTavish, D.** and **Hugues, P.**, *Finite Element Modeling of Linear Viscoelastic Structures*, ASME Biennal Conference on Mechanical Vibration and Noise, sep 1987.

[7] **Lesieutre, G.** and **Mingori, D.**, *Finite Element Modeling of Frequency-Dependent Material Damping Using Augmenting Thermodynamic Fields*, J. Guidance Control and Dynamics, Vol. 13, No. 6, pp. 1040–1050, 1990.

[8] **Balmès, E.**, Structural Dynamics Toolbox 3.1 (for use with MATLAB), Scientific Software Group, Sèvres (France), info@sdtools.com, 1998.

[9] **Plouin, A.** and **Balmès, E.**, *A Test Validated Model of Plates with Constrained Viscoelastic Materials*, IMAC, 1999.

[10] **Caughey, T.**, *Classical Normal Modes in Damped Linear Dynamic Systems*, ASME J. of Applied Mechanics, pp. 269–271, 1960.

[11] **Liang, Z., Tong. M., L.** and **G.C.**, *Complex Modes in Damped Linear Dynamic Systems*, Int. J. Anal. and Exp. Modal Analysis, Vol. 7, No. 1, pp. 1–20, 1992.

[12] **Balmès, E.**, *Model Reduction for Systems with Frequency Dependent Damping Properties*, IMAC, 1997.

[13] **Plouin, A.** and **Balmès, E.**, *Pseudo-Modal Representations of Large Models with Viscoelastic Behavior*, IMAC, pp. 1440–1446, 1998.

[14] **SOLLAC**, *Master curve of Solconfort-TA polymer*, Private communication, 1998.